journal of the mechanical behavior of biomedical materials 162 (2025) 106824

Contents lists available at ScienceDirect

Journal of the Mechanical Behavior of Biomedical Materials

journal homepage: www.elsevier.com/locate/jmbbm

Exploring the effect of displacement rate on the mechanical properties of denticulate ligaments through uniaxial tensile testing

Audrey Berriot [a,b,c], Morgane Evin [a,c], Karim Kerkouche [b,c], Elisabeth Laroche [b,c], Eva Gerard [b,c], Eric Wagnac [b,c,*]

[a] Aix Marseille Univ, Univ Gustave Eiffel, LBA, Marseille, France
[b] Ecole de Technologie Supérieur de Montréal, Montréal, Canada
[c] iLabSpine, Canada

ARTICLE INFO

Keywords:
Denticulate ligament
Mechanical properties
Constitutive modelling
pia mater
Dura mater

ABSTRACT

Denticulate ligaments play a key role in stabilizing the spinal cord (SC). Accurate representation of these structures in finite element modelling, whether in quasi-static or dynamic conditions, is essential for providing biofidelic responses. Therefore, understanding, characterizing and comparing the tensile mechanical properties of denticulate ligaments at different loading velocities is crucial. A total of 38 denticulate ligament samples at different cervical levels (anatomical levels from C1 to C7) were obtained from 3 fresh porcine SCs and 86 uniaxial tensile tests were performed immediately after dissection using an electro-mechanical testing system equipped with a 22 N loadcell. The mechanical tests included 10 cycles of preconditioning and a ramp with displacement rates of 0.1 mm s^{-1}, 1 mm s^{-1} and 10 mm s^{-1}. Bilinear piecewise fitting and trilinear piecewise fitting were performed to determine the elastic modulus and maximum stress and strainof the samples. While no significant differences in the mechanical behavior of the denticulate ligaments were found across the different displacement rates, notable variations were found between spinal levels, with a significantly higher elastic modulus at the lower cervical levels.

1. Introduction

The spinal cord (SC) plays a crucial role in transmitting signals from the brain to the body. In cases of SC trauma, complex stress distribution affect both the white matter and grey matter, resulting in the disruption of neural pathways and a significant loss of mobility and vital bodily functions. Spinal Cord Injuries (SCI) have a profound impact on the quality of life and life expectancy of patients, with the majority of injuries occurring at the cervical level (Jackson et al., 2004). The global incidence of SCI due to traumatic causes was 10.5 new cases per 100,000 persons per year between 2000 and 2016 (Kumar et al., 2018).

Enhanced mobility renders the cervical segment more prone to injuries with significant repercussions on bodily functions. The degree of SC mobility varies according to its location, with the cervical level showing greater mobility in comparison to other segments of the SC (Rycman et al., 2022).

In the event of an impact, the SC can be affected. The SC is attached within the spinal canal by the nerve roots and is anchored at both ends. Additionally, the denticulate ligaments (DL) contribute to its stabilization within the vertebral canal (Tubbs et al., 2001). DL are thin hourglass-shaped structures that connect the pia mater and the dura mater within the subarachnoid space of the vertebral canal. Extensive research have shown that DL play a crucial role on the stabilization of the SC in all directions (Bilston and Thibault, 1995; Parkinson, 1991; Tubbs et al., 2001), preventing excessive stretching and strain on spinal nerve roots during traumatic events (Ceylan et al., 2012; Tubbs et al., 2001). In human, approximatively 20 DL can be found along the SC, extending from the cranio-vertebral junction to the T12 vertebra. Histological examination has revealed that the DL are composed of collagen fiber bundles. Notably, at the cervical levels, the collagen fibers of the DL penetrate the substance of the SC at different intervals, creating a stronger attachment. Comparatively, the cervical DL exhibit thicker and more abundant collagen fibers than the thoracic DL (Ceylan et al., 2012), emphasizing the importance of studying the mechanical properties of the denticulate ligaments in this area.

Finite element simulations have demonstrated that stress distribution in the SC serves as a valuable indicator of damage severity (Erbulut

* Corresponding author. Département de génie mécanique, École de technologie supérieure, Université du Québec, 1100, rue Notre-Dame Ouest, bureau A-2818, Montréal, Québec, H3C 1K3, Canada.
E-mail address: eric.wagnac@etsmtl.ca (E. Wagnac).

https://doi.org/10.1016/j.jmbbm.2024.106824
Received 1 June 2024; Received in revised form 17 November 2024; Accepted 18 November 2024
Available online 19 November 2024

Abbreviations

DAC	Dura mater and arachnoid complex
DL	Denticulate Ligament(s)
SC	Spinal Cord
SCI	Spinal Cord Injuries

offering initial values for modeling purposes. However, there is currently no available information on the non-linear mechanical response of DL at higher strain rates or on how changes in mechanical properties of DL occur under different loading conditions. For instance, providing mechanical properties of these structures at higher displacement rates is essential for creating biofidelic and accurate numerical models of the spine. This enhancement would improve our ability to study physiological phenomena and enhance our trauma prediction capabilities.

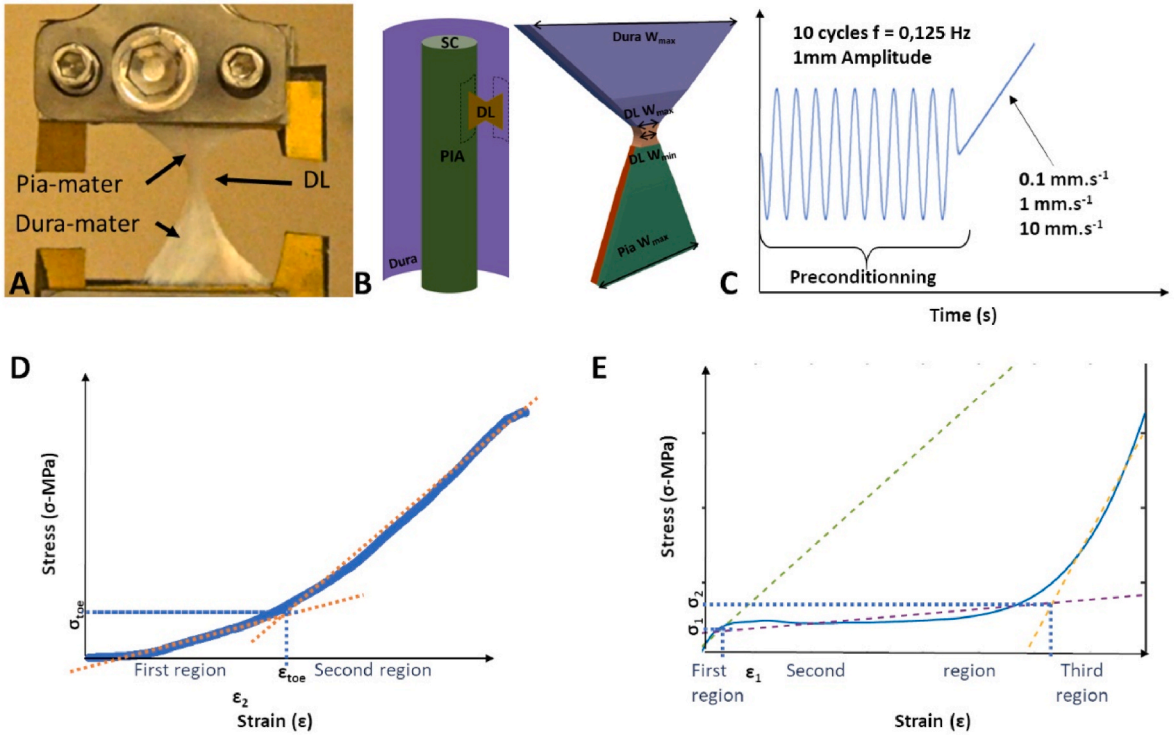

Fig. 1. A) Typical sample of a denticulate ligament, along with the pia and dura mater, mounted in clamps in the experimental testing machine. The denticulate ligament lies between the pia mater and the dura mater B) 3D representation of the denticulate ligament, within the canal and in test condition showing its minimum and maximum width C) Tensile test protocol including a cyclic preconditioning and a tensile test at a constant displacement rate D) bilinear and E) trilinear stress-strain curves of all samples.

et al., 2014; Greaves et al., 2008; Singhal et al., 2023), a finding that has been corroborated by clinical data from patients (Czyz et al., 2016). Additionally, localized areas of tensile and compressive strains due to DL were reported from 3T MRI strain field acquisitions in 19 participants during quasi-static motions such as flexion and extension (Stoner et al., 2019). Beauséjour et al. (2022) also reported local compression and distraction at the DL attachment points. Considering the role of DL in SC stabilization, their inclusion into finite element models becomes crucial for achieving a more realistic representation of the SC behavior, whether in quasi-static or dynamic studies. Furthermore, their inclusion opens broader possibilities, including the ability to predict local stress distribution that may lead to SC injury or occur during surgical procedures. These advancements hold promise for the development of predictive spinal injury models and surgical planning tools, offering valuable insights for a range of applications.

But obtaining accurate mechanical properties of the DL to incorporate into finite element models is a significant challenge for improving our understanding and modeling of SC biomechanics. Previous studies have conducted quasi-static (0.03 mm.s^{-1} i.e., approximatively 0.01 s^{-1}) tensile tests to provide mechanical characterization of these structures at the cervical level. The reported average elastic moduli were 2.1 MPa (Polak et al., 2014) and 3.8 MPa (Polak-Kraśna et al., 2019),

The effect of strain rate on the mechanical properties of soft tissues has been previously studied across a variety of soft tissues (Fung, 1984; Avril et al., 2013; Tran and Tsai, 2023; Kang et al., 2023). Generally, an increase in strain rate tends to result in a steeper slope in stress-strain curves, indicating higher stiffness (Marino, 2018). In a specific study on the viscoelastic response of aortic valve tissue, the viscoelastic content parameter showed a slight increase with strain rates, while the time constants remained unaffected by changes in strain rate (Doehring et al., 2004).

This study aims to mechanically characterize and compare the tensile mechanical properties of DL at different displacement rates (0.1 mm s^{-1}, 1 mm s^{-1} and 10 mm s^{-1}) across various locations using porcine cervical spines. The investigation will focus on the variability of the DL's material properties within the cervical spine and the influence of strain rates on those material properties. By investigating the behavior of DL under various loading conditions, this research seeks to provide valuable insights into their mechanical response and contribute to a deeper understanding of their biomechanical properties.

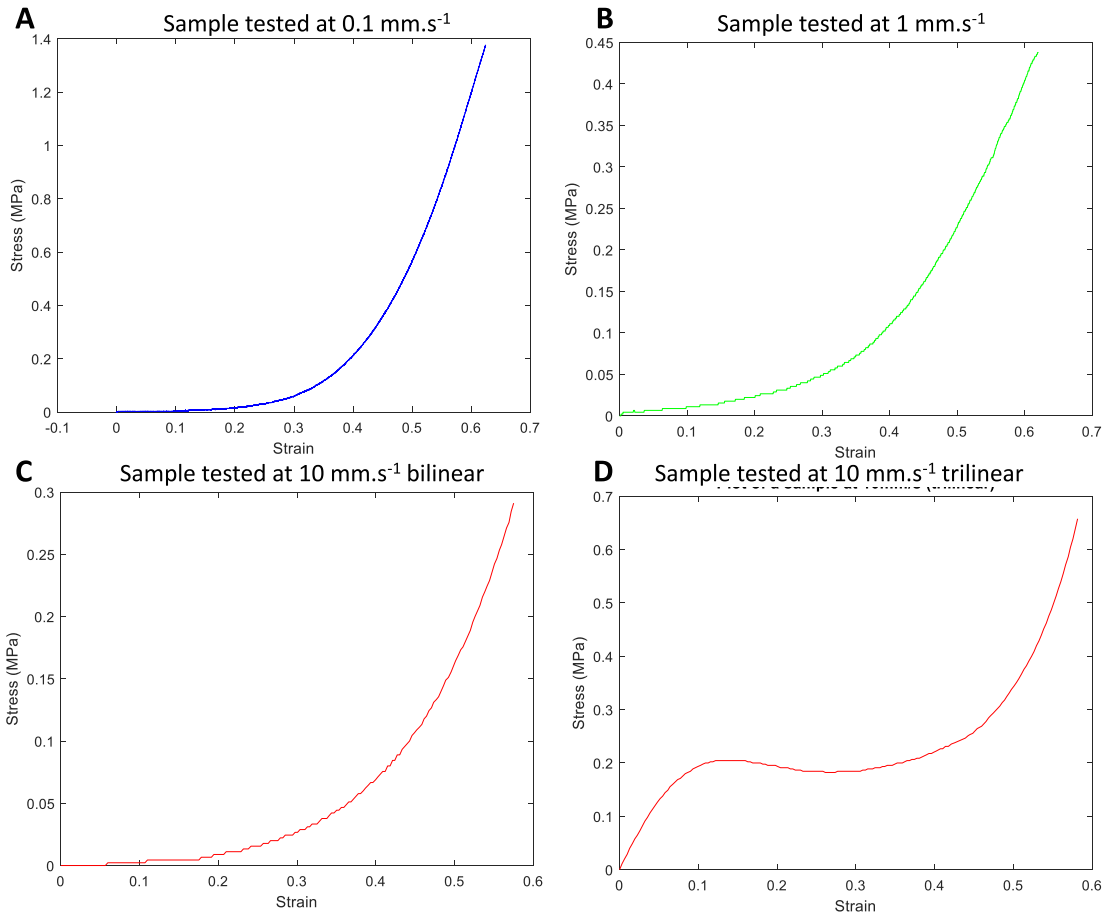

Fig. 2. Stress-strain curves from mechanical tensile testing of denticulate ligaments A) Typical curve at 0.1 mm s^{-1} B) Typical curve at 1 mm s^{-1} C) Typical curve at 10 mm s^{-1} (bilinear behavior) D) Typical curve at 10 mm s^{-1} (trilinear behavior).

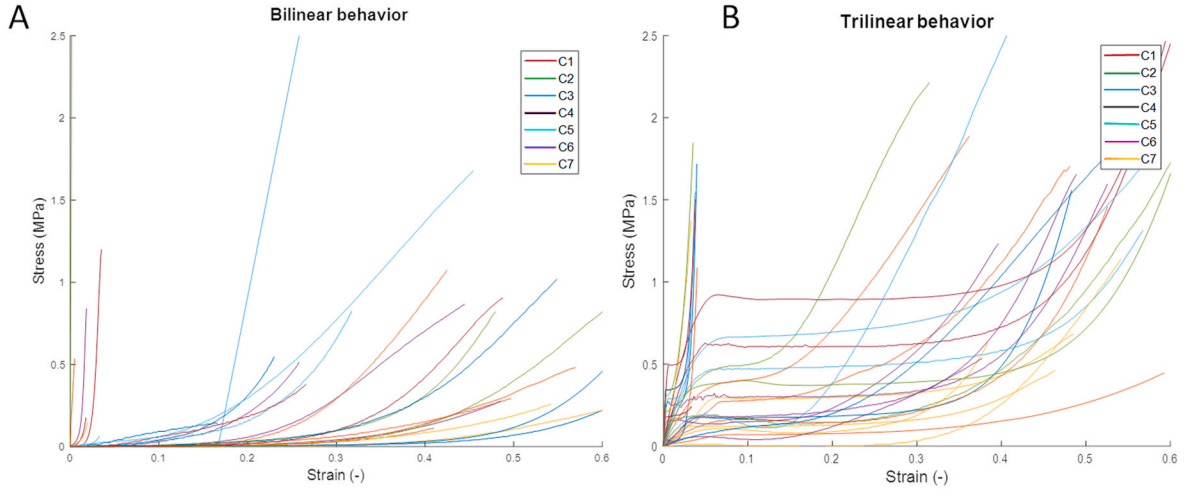

Fig. 3. Stress-strain curves of all ligament samples. A) Bilinear response and B) trilinear response.

2. Materials and methods

2.1. Sample preparation

Three fresh cervical SCs were harvested from 4-month-old pigs weighing between 30 and 43 kg within 3 h of the animal's sacrifice. All samples were obtained post-mortem from previous experiments that did not affect spinal cord physiology ('CM21025NNp' protocol) and were conducted in accordance with the Good Animal Practice (GAP) guidelines from the Canadian Council on Animal Care (CCAC). Extraction took place at the Research Centre of the CHUM (Centre Hospitalier de l'Université de Montréal, with certification from the CCAC issued on March 6, 2020. The dura mater and arachnoid complex (DAC) was incised to expose the DLs with the pia mater, and the pia mater was cut

Table 1
Average DL material properties by cervical spine levels and displacement 410 rates. Etoe and E2: modulus measured in the first (toe) region of the bilinear curves and in the second region of the trilinear curves, respectively. EElastic and E3: modulus measured in the second (elastic) region of the bilinear curves and in the third region of the trilinear curves, respectively; εtoe and ε2: strain values at the transition between the first and second regions of the bilinear curves, and between the second and third regions of the trilinear curves, respectively; σtoe and σ2: stress values at the transition between the first and second regions of the bilinear curves, and between the second and third regions of the trilinear curves, respectively. Ogden model coefficients are noted as μ1 and α1, r^2 and RMSE are errors calculations.

Displ.rate (mm. s^{-1})	Level	N	E_{toe} and E_2 (MPa)	$E_{Elastic}$ and E_3 (MPa)	ε_{toe} and ε_2	σ_{toe} and σ_2 (MPa)	Ogden Model			
							μ_1	α_1	r^2	RMSE
0.1	Total	27	0.80 ± 1.27	8.58 ± 8.20	0.39 ± 0.12	1.01 ± 1.02	0.01 ± 0.01	22.73 ± 29.99	1 ± 0	0.05 ± 0.09
	C1	3	1.03 ± 0.39	11.24 ± 10.33	0.27 ± 0.22	0.88 ± 0.48	0.02 ± 0.02	45.39 ± 58.60	0.99 ± 0.01	0.18 ± 0.28
	C2	3	0.15 ± 0.13	2.42 ± 1.71	0.47 ± 0.07	0.13 ± 0.11	0 ± 0	14.17 ± 4.28	0.99 ± 0	0.03 ± 0.04
	C3	6	0.36 ± 0.37	4.60 ± 5.21	0.43 ± 0.03	0.88 ± 1.17	0 ± 0.01	14.12 ± 3.85	1 ± 0	0.03 ± 0.04
	C4	5	1.97 ± 2.76	14.10 ± 14.75	0.33 ± 0.18	0.89 ± 0.30	0.01 ± 0.02	39.64 ± 55.08	1.00 ± 0.01	0.03 ± 0.01
	C5	6	0.56 ± 0.22	8.95 ± 4.70	0.45 ± 0.05	1.19 ± 1.11	0 ± 0	15.64 ± 2.61	1 ± 0	0.05 ± 0.03
	C6	3	0.67 ± 0.17	9.76 ± 3.48	0.37 ± 0.13	2.23 ± 1.73	0.02 ± 0.02	14.77 ± 4.1	0.99 ± 0	0.06 ± 0.04
	C7	1	0.73	9.54	0.42	0.75	0.01	14.08	1	0.06
1	Total	23	0.71 ± 0.53	8.46 ± 4.72	0.32 ± 0.18	0.95 ± 1.19	0.01 ± 0.02	51.97 ± 71.66	0.99 ± 0.01	0.03 ± 0.03
	C1	3	1.33 ± 1.05	7.83 ± 2.37	0.03 ± 0.01	0.09 ± 0.07	0 ± 0	162.1 ± 51.1	0.97 ± 0.04	0 ± 0
	C2	3	0.44 ± 0.23	8.10 ± 4.36	0.46 ± 0.07	0.45 ± 0.41	0 ± 0	19.84 ± 6.62	1 ± 0	0.02 ± 0.02
	C3	6	0.43 ± 0.4	5.98 ± 4.9	0.3 ± 0.17	0.43 ± 0.33	0.01 ± 0.02	47.74 ± 84.36	0.99 ± 0	0.03 ± 0.04
	C4	4	0.82 ± 0.57	7.23 ± 4.93	0.3 ± 0.21	0.41 ± 0.40	0.01 ± 0.01	59.67 ± 89.35	1 ± 0	0.03 ± 0.03
	C5	4	0.73 ± 0.17	12.56 ± 6.04	0.46 ± 0.06	2.00 ± 0.86	0 ± 0.01	17.44 ± 3.74	1 ± 0	0.04 ± 0.04
	C6	2	0.81 ± 0.36	11.97 ± 0.11	0.37 ± 0.25	2.07 ± 2.39	0.01 ± 0.01	21.96 ± 1.78	0.99 ± 0	0.04 ± 0.01
	C7	1	1.55	13.05	0.4	0.44	0.03	14.67	1	0.06
10	Total	36	0.59 ± 1.19	8.66 ± 7.97	0.30 ± 0.13	0.45 ± 0.39	−2.49 ± 7.92	31.93 ± 77.8	0.81 ± 0.47	0.08 ± 0.08
	C1	6	1.12 ± 1.19	13.22 ± 15.35	0.34 ± 0.16	0.37 ± 0.46	0.01 ± 0.02	54.6 ± 101.1	1 ± 0	0.08 ± 0.16
	C2	7	0.37 ± 0.30	4.56 ± 2.16	0.31 ± 0.12	0.38 ± 0.28	−3.57 ± 9.52	12.89 ± 9.04	0.71 ± 0.74	0.05 ± 0.03
	C3	5	0.31 ± 0.32	3.79 ± 2.15	0.26 ± 0.11	0.15 ± 0.07	−1.4 ± 3.24	9.52 ± 6.28	0.89 ± 0.23	0.06 ± 0.04
	C4	6	0.60 ± 0.43	9.65 ± 4.49	0.33 ± 0.15	0.35 ± 0.29	0 ± 0	86.8 ± 160.7	0.83 ± 0.29	0.05 ± 0.03
	C5	4	0.65 ± 0.38	7.81 ± 1.72	0.38 ± 0.06	0.43 ± 0.21	0.00 ± 0.01	21.32 ± 5.95	0.98 ± 0.02	0.06 ± 0.02
	C6	4	1.56 ± 1.85	13.33 ± 9.68	0.23 ± 0.14	0.89 ± 0.38	−6.3 ± 13.0	10.44 ± 7.30	0.64 ± 0.69	0.13 ± 0.02
	C7	4	−0.48 ± 2.51	9.81 ± 7.01	0.27 ± 0.11	0.78 ± 0.6	−8.1 ± 16.4	9.14 ± 6.52	0.61 ± 0.75	0.14 ± 0.08

to expose and remove the grey and white matter. To collect DL samples, square-shaped incisions were made in the pia and dura maters. Accordingly, a DL sample was composed of a complete DL ligament with parts of pia mater and dura mater at its extremities (Fig. 1A). DL samples were immediately stored in a saline solution at 20 °C after dissection and kept in this solution for less than 4 h before testing. Prior to testing, they were removed from the saline solution, gently dried with paper, and positioned in the holding system. Fragments of the pia and dura mater were folded and used to clamp samples in the tensile test machine (Fig. 1A). Sandpaper was used at the interface between the upper and lower jaws and the samples to avoid slippery. Once clamped, samples had an hourglass shape. To prevent drying, they were sprayed with saline solution after being secured in the system. The dimensions of each sample were measured using a Mitutoyo Absolute Digimatic caliper (model 500-196-30 – accuracy of ±0.02 mm; Mitutoyo, USA) after the sample had swollen, while it was in the holding system, following the application of a 0.1 N preload. Measured dimensions included the total sample length (L_T), the individual lengths of the pia mater (L_{PM}), the dura mater (L_{DM}) and the denticulate ligament (L_{DL}), as well as the width (w). Due to the slight hourglass shape of the DL, its width was calculated as the average of the maximum and minimum ligament width measurements (Fig. 1B). Measuring the DL thickness proved to be challenging and could not be performed for all samples. Therefore, we used the average DL thickness values per cervical level from Polak et al. (2014), ensuring that our measurements - though difficult to replicate – were consistent with the reported range.

2.2. Tensile test protocol

Uniaxial tensile tests were performed on an electro-mechanical testing system (Bose ElectroForce 3200, Bose, United-States, displacement range 0.002–13 mm and frequency range 0.0001–300 Hz) equipped with a 22 N load cell (maximum error for accuracy: ±0.15 % of the full scale for non-linearity and hysteresis and ±0.05 % of the full scale for non-repeatability). Each specimen was stretched to a preload force of 0.1 N to remove any folds and enable dimensional measurements. Then,

Table 2
Average DL material properties for samples exhibiting a trilinear response. – E1 and E2: modulus measured in the first region and in the second region of the trilinear curves, respectively. E3: modulus measured in the third region of the trilinear curves, respectively; ε1 and ε2: strain values at the transition between the second and third regions of the trilinear curves, respectively; σ1 and σ2: stress values at the transition between the second and third regions of the trilinear curves, respectively. "±" represent standard deviations.

Displ. rate (mm.s^{-1})	Level	N	E_1 (Mpa)	E_2 (MPa)	E_3 (MPa)	ε_1	σ_1 (MPa)	ε_2	σ_2 (MPa)
0.1	Total	19	20.13 ± 27.91	1.09 ± 1.60	13.45 ± 21.19	0.05 ± 0.04	1.06 ± 1.07	0.36 ± 0.16	1.3 ± 1.08
	C1	2	56.02	1.23	5.29	0.05	0.95	0.17 ± 0.19	1.1
	C2	2	1.11 ± 1.44	0.17 ± 0.17	2.6 ± 2.37	0.04 ± 0	0.05 ± 0.05	0.43 ± 0.04	0.14 ± 0.15
	C3	3	7.33 ± 6.73	0.3 ± 0.2	5.56 ± 6.67	0.07 ± 0.05	1.24 ± 1.58	0.43 ± 0.04	1.42 ± 1.50
	C4	4	34.99 ± 29.20	2.92 ± 3.01	36.55 ± 41.17	0.02 ± 0.02	0.72 ± 0.29	0.2 ± 0.21	0.90 ± 0.33
	C5	5	9.87 ± 9.53	0.64 ± 0.14	10.05 ± 4.28	0.07 ± 0.04	1.05 ± 1.13	0.46	1.41 ± 1.09
	C6	2	27.26 ± 3.79	0.64 ± 0.23	8.55 ± 3.93	0.07 ± 0.02	2.91 ± 0.19	0.4 ± 0.16	3.22 ± 0.26
	C7	1	2.42	0.73	9.54	0.03	0.39	0.42	0.75
1	Total	17	17.15 ± 15.95	1.07 ± 1.33	16.18 ± 29.67	0.06 ± 0.04	1.09 ± 1.21	0.29 ± 0.19	1.31 ± 1.27
	C1	2	8.57 ± 7.20	1.67 ± 1.23	6.6 ± 1.49	0.01 ± 0	0.10 ± 0.05	0.03 ± 0.01	0.12± 0.06
	C2	1	5.39	0.58	12.98	0.1	0.59	0.46	0.92
	C3	4	17.22 ± 20.39	1.59 ± 2.69	34.11 ± 61.34	0.06 ± 0.05	0.53 ± 0.20	0.27 ± 0.20	0.64 ± 0.16
	C4	2	7.98 ± 6.99	0.77 ± 0.07	7.21 ± 2.35	0.02 ± 0.02	0.44 ± 0.50	0.14 ± 0.16	0.54 ± 0.61
	C5	4	19.13 ± 12.11	0.73 ± 0.17	12.56 ± 6.04	0.07 ± 0.04	1.59 ± 0.98	0.46 ± 0.06	2.00 ± 0.86
	C6	3	19.68 ± 19.90	0.81 ± 0.36	11.97 ± 0.11	0.07 ± 0.06	1.77 ± 2.27	0.37 ± 0.25	2.07 ± 2.39
	C7	1	51.05	0.72	7.71	0.06	3.77	0.23	3.95
10	Total	21	5.02 ± 5.31	0.52 ± 1.48	8.88 ± 7.5	0.07 ± 0.03	0.40 ± 0.48	0.28 ± 0.14	0.54 ± 0.42
	C1	2	7.43 ± 10.06	1.45 ± 1.77	17.34 ± 17.01	0.03 ± 0.04	0.06 ± 0.05	0.20 ± 0.24	0.15 ± 0.03
	C2	4	4.59 ± 2.83	0.37 ± 0.41	4.57 ± 2.84	0.1 ± 0.01	0.47 ± 0.32	0.33 ± 0.14	0.56 ± 0.23
	C3	2	2.01 ± 0.85	0.24 ± 0.47	3.53 ± 2.01	0.08 ± 0	0.17 ± 0.07	0.20 ± 0.01	0.22 ± 0
	C4	3	1.61 ± 1.47	0.41 ± 0.43	9.37 ± 4.77	0.05 ± 0.04	0.11 ± 0.09	0.26 ± 0.22	0.27 ± 0.31
	C5	4	2.07 ± 1.55	0.65 ± 0.38	7.81 ± 1.72	0.06 ± 0.01	0.16 ± 0.13	0.38 ± 0.06	0.43 ± 0.21
	C6	3	9.43 ± 1.26	1.69 ± 2.24	12.82 ± 11.79	0.09 ± 0.03	0.90 ± 0.24	0.24 ± 0.16	1.08 ± 0.03
	C7	3	8.94 ± 10.45	−0.97 ± 2.83	9.57 ± 8.56	0.07 ± 0.02	0.78 ± 1.04	0.24 ± 0.12	0.88 ± 0.69

Table 3
Dimensions, meshing and material properties of the FEMs.

Level	Dimensions (mm)				Nb of elements	Nb of nodes	Material properties			
	Parameter	Dura	Pia	DL			Dura	Pia	DL	
C2	t	0.56	0.44	0.33	13641	31016	$\mu_1 = 0.0050$	$\mu_1 = 0.0042$	0.1 mm s^{-1}	$\mu_1 = 0.0001$
	w_{max}	8.33	6.71	1.20			$\alpha_1 = 11.93$	$\alpha_1 = 9.01$		$\alpha_1 = 26.18$
	w_{min}	1.20	1.20	1.16					1 mm s^{-1}	$\mu_1 = 0.0007$
	l	1.85	3.98	0.83						$\alpha_1 = 216.67$
C7	t	0.56	0.44	0.32	16865	37347			0.1 mm s^{-1}	$\mu_1 = 0.024$
	w_{max}	5.74	3.02	0.58						$\alpha_1 = 13.97$
	w_{min}	0.58	0.58	0.41					1 mm s^{-1}	$\mu_1 = 0.0024$
	l	2.20	2.85	0.45						$\alpha_1 = 190.75$

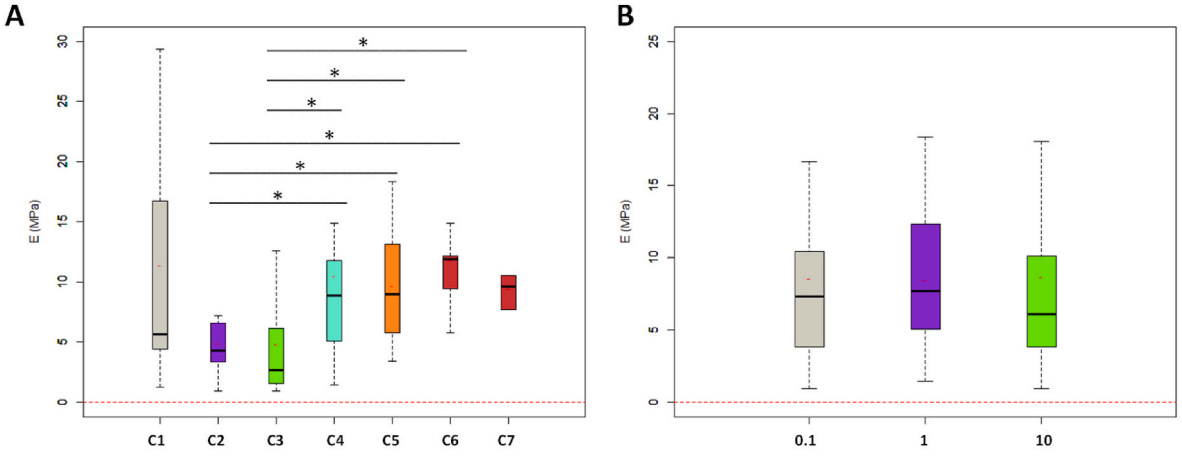

Fig. 4. A) Box plot of the elastic modulus, defined as the second slope in bilinear curves and as the third slope in trilinear curves, for all displacement rates, grouped by cervical level B) Box plot of the elastic modulus for all cervical levels, grouped by displacement rates.

10 cycles of preconditioning at a frequency of 0.125 Hz (elongation of 1 mm, displacement rate of 0.25 mm s^{-1}). and a ramp of 0.1 mm s^{-1}, 1 mm s^{-1} or 10 mm s^{-1} were performed until a displacement of 2 mm (32.7 ± 4.1% of the total length in average) of the upper jaw was reached. These loading conditions were established based on preliminary uniaxial tensile-to-failure tests performed on cervical samples at a displacement rate of 0.1 mm s^{-1}. A typical force-displacement curve of a tensile-to-failure test is provided in Supplementary data 2. DL

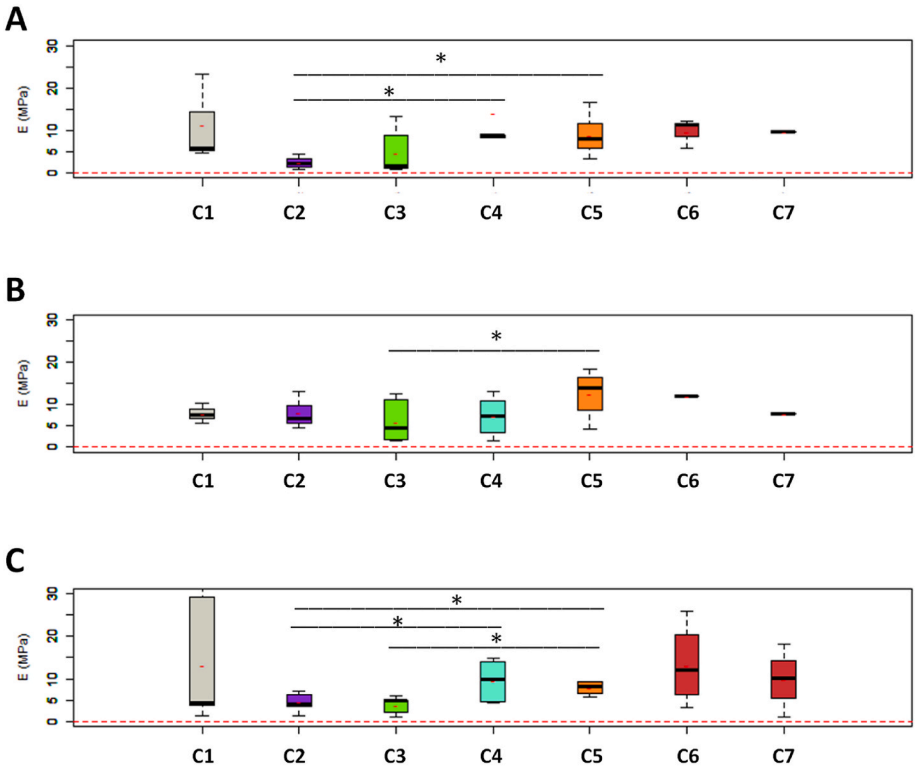

Fig. 5. Box plot showing the elastic modulus, defined as the second slope in bilinear curves and as the third slope in trilinear curves, per cervical level A) at 0.1 mm s^{-1} B) at 1 mm s^{-1} and C) 10 mm s^{-1}.

samples were immediately stored in a saline solution at 20 °C after dissection and kept in this solution for he displacement rates were selected to allow for comparison with previously published quasi-static data by Polak et al. (2014) (2 mm min^{-1}, 0.033 mm s^{-1}) while also being sufficiently high to reach dynamic conditions. Each specimen underwent tensile testing at the selected displacement rates in a randomized order. Throughout each test, displacement of the upper jaw and tensile force were recorded as functions of time. Additionally, a video camera (Sony Handycam HDR-CX405, Sony, Tokyo, Japan) was set perpendicular to the test system in order to capture video footage of all tensile tests at a frequency of 30 fps.

2.3. Post-processing

Engineering stress-strain curves were generated for the DL part of the sample only. The initial cross section area A_0 used for calculating the engineering stress was determined according to the following formula (equation (1)):

$$A_0 = w^* t \tag{1}$$

where w and t represent the width and thickness of the DL sample, respectively (Fig. 1 B). The dimensions of the DL samples for each cervical level are provided in Supplementary Data 1.

The engineering stress was determined by dividing the force measured by the load cell with the initial cross-sectional area (A_0) of the denticulate ligament (equation (2)). This assumes that the displacement applied to the sample generates a uniform force across the pia mater, the dura mater, and the denticulate ligament. This hypothesis was subsequently validated through finite element modeling (as discussed in the next section). To determine the elongation of each DL (ΔL_{DL}), the DL elongation relative to the total elongation of the sample ($\Delta L_{DL}/\Delta L_T$) during the test was monitored by video acquisition (Fig. 1-A). Virtual markers were placed on the clamps and the DL extremities, and semi-automatically tracked using GOM Correlate software (Zeiss GOM Metrology, Braunschweig, Germany). The ratio of DL elongation to total sample elongation ($\Delta L_{DL}/\Delta L_T$) observed on the (uncalibrated) video during the test was then used to compute the DL elongation, by multiplying this ratio by the displacement of the upper clamp, which corresponds to the total sample elongation (equation (3)). The engineering strain was calculated by dividing the DL elongation by the initial length of the DL (equation (4)).

$$\sigma_0 = \frac{F}{A_0} \tag{2}$$

$$\Delta L_{DL} = \left(\frac{\Delta L_{DL}}{\Delta L_T}\right) * \Delta L_T \tag{3}$$

$$\varepsilon_{DL} = \frac{\Delta L_{DL}}{L_{DL}} \tag{4}$$

The resulting stress-strain curve for each DL sample was analyzed using a bilinear or trilinear fitting algorithm in Matlab R2022 (Mathworks, Natick, USA), optimizing for the maximum r^2 value across all linear segments (Evin et al., 2022). For each curve, two or three moduli of elasticity (slopes) were calculated based on whether two or three distinct regions could be identified (Fig. 1C–D, Fig. 2). Additionally, the stresses (σ) and the strains (ε) at specific points were determined: after the first region (σ_1 and ε_1) and between the second and final regions (σ_2 and ε_2). The quality of fit was assessed using r^2, and the elastic modulus of the sample was computed as the slope of the elastic region which corresponds to be the second slope in bilinear behavior and the third slope in trilinear behavior.

A first-order Ogden constitutive model was also fitted to the stress-strain curves, following the approach of (Berriot et al., 2023), which defines the strain energy density function of the material as:

$$\psi_{Ogden} = \sum_{i=1}^{n} \frac{\mu_i}{\alpha_i} \left(\lambda_1^{\alpha_i} + \lambda_2^{\alpha_i} + \lambda_3^{\alpha_i} - 3\right) \tag{5}$$

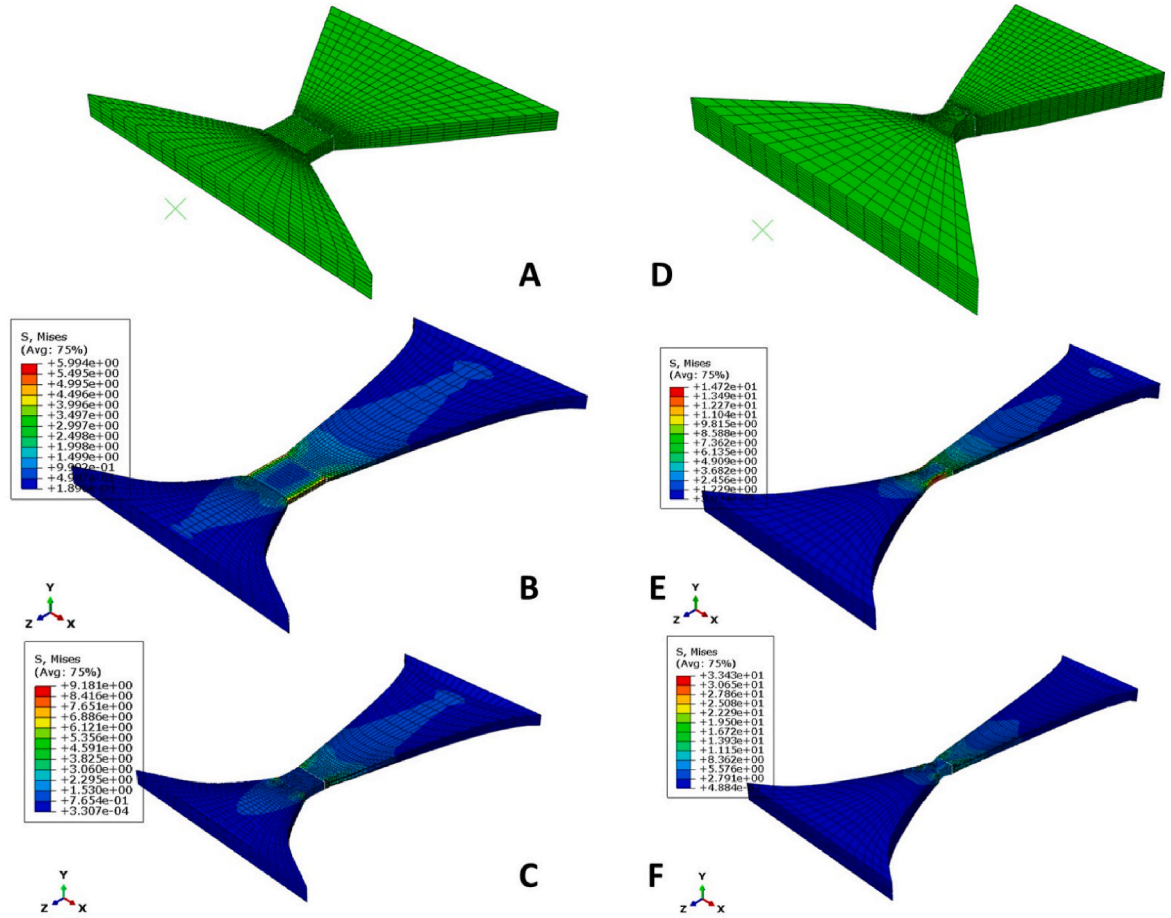

Fig. 6. A) FEM of the C2 complete sample B) Von Mises stress (MPa) showing higher stress in the C2 DL ligament at 0.1 mm.s-1 C) Von Mises stress (MPa) in C2 DL ligament at 1 mm.s-1 D) FEM of the C7 complete sample E) Von Mises stress (MPa) showing high stress in the C7 DL ligament at 0.1 mm.s-1 F) Von Mises stress (MPa) in C7 DL ligament at 1 mm.s-1.

where λ_i are principal stretches and α_i, μ_i are material coefficients for n = 1.

All curve analyses were performed with a custom-made Matlab algorithm (Matlab version 2022, Matworks, Naticks, USA).

2.4. Finite element modeling of the tensile test

Finite element models (FEMs) of complete C2 and C7 samples were developed using Abaqus software (version 6, Dassault Systèmes, France) to test the hypothesis that the displacement applied to the sample generated a uniform force across the pia mater, dura mater and denticulate ligament, as if they acted as non-linear springs in series. The geometry of these FEMs represents two specific samples selected from the entire dataset. Figures of the FEMs, along with detailed information on the models' dimensions, meshing and material properties are provided in Table 3. In summary, the thickness of the pia mater and the dura mater was taken from Sudres et al. (2021) and then doubled to account for the presence of both the upper and lower layers surrounding the denticulate ligament (DL) after extraction (Fig. 1B), and that were folded to fix the sample in the clamps. The folding of the pia and dura maters materials was reproduced in the model, ensuring that both the top and bottom layers of each membrane are well represented."The samples were meshed using eight-node brick elements, with the mesh size chosen based on a convergence study to balance accuracy and computing time. A hyperelastic material model based on a first-order Ogden formulation was used to simulate the mechanical behavior of the three components of the sample. The Ogden coefficients for the pia and dura mater were taken from Sudres et al. (2021), while the coefficients of the DL were derived from this study and adjusted according to the applied displacement rates. All nodes at the bottom of the FEMs were fixed to simulate the attachment of the sample to the stationary bottom clamp. Displacement rates of 0.1 and 1 mm s^{-1} were applied to the upper nodes of the FEMs to simulate the moving clamp, up to a displacement of 2 mm.

2.5. Statistical analysis

Data were analyzed using R statistical software (R Core Team, 2020). The normality of the data was assessed using a Shapiro-Wilk test. Subsequently, a Kruskal-Wallis rank test was employed to ascertain the significance of variations in the mechanical properties of denticulate ligaments with respect to displacement rates and spinal levels (C1 to C7). A significance level was depicted as '*' for $p \leq 0.05$.

Boxplots were used to visually represent the elastic modulus across different strain rates and spinal levels. They display the median, interquartile range and whiskers, which indicate the 25th and 75th percentiles. A hyphen marks the mean value of the variable being depicted.

Mechanical testing results were classified into two groups based on their behavior: either bilinear or trilinear. Receiver operating characteristic (ROC) analysis was performed to determine a displacement rate threshold that could potentially induce a shift in behavior from bilinear to trilinear. This analysis was carried out using the pROC library in R.

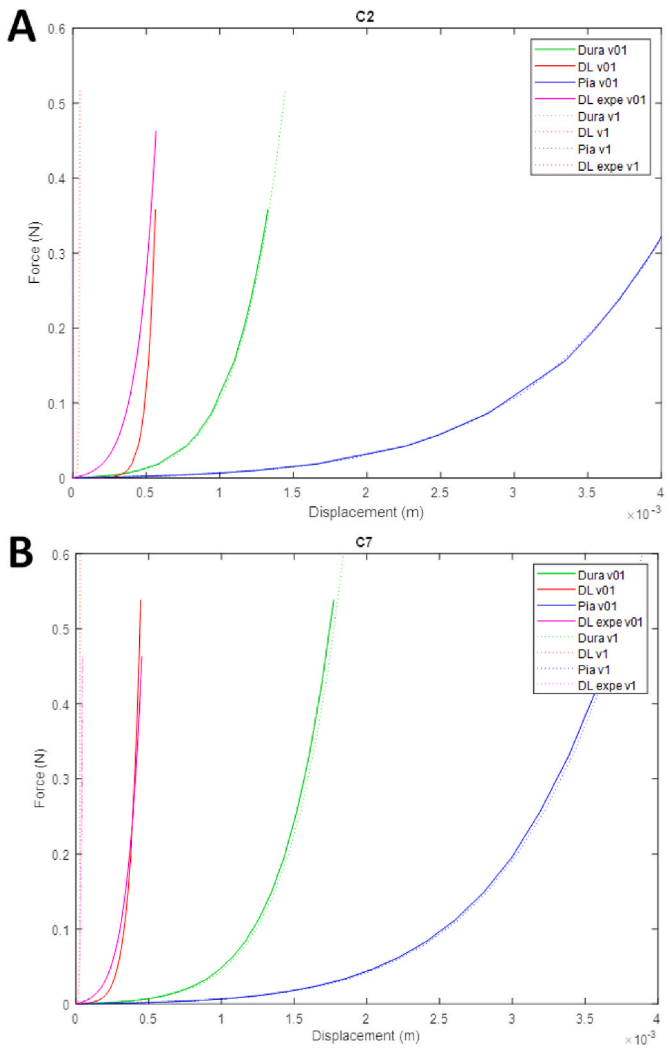

Fig. 7. Simulated vs experimental stress-elongation (lambda) curves observed on the complete samples A) C2 sample at 0.1 mm s^{-1} and C2 sample at 1 mm s^{-1} B) C7 sample at 0.1 mm s^{-1} and C7 sample at 1 mm s^{-1}.

3. Results

A total of 38 samples were obtained and tested within 12 h of extraction, resulting in 114 tensile tests (3 tests per sample). However, 28 tests were excluded from the results due to invalid force data, likely caused by improper sample fixation or slippage at the clamp interface, as confirmed by video analysis. No damage to the samples was observed during testing. Ultimately, 27 tests were considered acceptable at a displacement rate of 0.1 mm s^{-1}, 23 at 1 mm s^{-1} and 36 at 10 mm s^{-1}. The corresponding strain rates applied to the complete samples were 0.61 ± 0.08 s^{-1}, 6.26 ± 0.86 s^{-1}, 62.6 ± 8.6 s^{-1}, for displacement rates of 0.1 mm s^{-1}, 1 mm s^{-1} and 10 mm s^{-1}, respectively. The corresponding DL strain rate, once corrected with DL elongations, were: 0.03 ± 0.01 s^{-1} for displacement rate of 0.1 mm s^{-1}, 0.27 ± 0.09 s^{-1} for 1 mm s^{-1} and 2.92 ± 1.41 s^{-1} for 10 mm s^{-1}.

After preconditioning, a toe region was observed in bilinear curves (Fig. 2A-C, Fig. 3-A), followed by a linear region. Trilinear curves (Fig. 2-D, Fig. 3-B) were observed for all displacement rates: 70.4% at 0.1 mm s^{-1}, 73.9% at 1 mm s^{-1} and 58.3% at 10 mm s^{-1}. On average, the proportion of trilinear curves across all displacement rates was 66.3%. In trilinear curves, a linear elastic region was first observed, followed by a plateau region and a second linear region.

The results of the analysis for all curves (Fig. 1-C) are displayed in Table 1, while the analysis of trilinear curves only (Fig. 1-D, Fig. 2-D, Fig. 3-B) are displayed in Table 2. No significant difference was found when comparing the second bilinear slope to the third trilinear slope.

No significant differences in material properties (elastic modulus and toe region modulus) were found between the displacement rates, even when analyzed separately for each cervical level (Fig. 4). However, elastic moduli showed significant differences between certain cervical levels (C2 and C3 compared to C4, C5, and C6) when all three displacements rates were considered together ($p < 0.05$). Additionally, significant differences were noticed between cervical levels when tested at specific displacement rates: between C2 and C5 (at 0.1 and 10 mm s^{-1}), between C2 and C4 and between C3 and C5 (at 10 mm s^{-1}; Fig. 5, $p < 0.05$).

ROC analysis identified a displacement rate threshold for the whole sample of 1.65 s^{-1} to distinguish between bilinear and trilinear behavior. This analysis demonstrated a sensitivity of 90.4 %, a specificity of 41.4 %, and an accuracy 72.8 % at this threshold.

The von mises stress in the FE DL models are depicted in Fig. 6 for both C2 and C7 models. Additionally, the simulated force-displacement curves for the complete samples were compared with those obtained experimentally under similar conditions, showing good agreement (RMSE values ranging from 0.02 to 0.06 N across the four simulations – Fig. 7). The forces acting on the pia mater, dura mater and DL were extracted from the simulation, confirming the hypothesis of uniform force distribution across these components (Supplementary Data 3). Additionally, the Von Mises stress distribution revealed that the highest stresses were concentrated in the DL.

4. Discussion

The aim of this study was to investigate potential differences in material properties of isolated denticulate ligaments across various displacement rates. The main findings are.

1) There were no significant differences in mechanical properties between displacement rates;
2) The identification of a strain rate threshold of 1.65 s^{-1}, which distinguishes between bilinear and trilinear behavior under tension, is a novel finding. However, this threshold only partially accounts for the observed changes in behavior.

Previous studies have exclusively focused on the quasi-static material properties of DL at a displacement rate of 2 mm min^{-1} (equivalent to 0.033 mm s^{-1}) along the porcine cervical spine (Polak et al., 2014; Polak-Kraśna et al., 2019). Similar to our study, their tensile tests were conducted on three materials in series: the pia mater, the DL, and the dura mater. However, they reported Young's moduli based on the initial length and elongation of the entire sample, which included the DL attached to both the pia mater and the dura mater (Polak et al., 2014). As a result, their findings reflect the combined mechanical properties rather than the isolated DL, as is the case in our study.

Despite the methodological differences, our results, which isolate the specific mechanical contribution of the DL, remain within the same order of magnitude as those reported in previous studies, providing confidence in the validity of our findings. For instance, Polak et al. (2014) and Polak et al. (2019) reported average quasi-static Young's moduli of 2.06 MPa and 3.81 MPa, respectively, at a displacement rate of 0.033 mm s^{-1}. In comparison, our study found average slopes of the second and third regions to be 5.98 MPa at a displacement rate of 0.1 mm s^{-1}, 7.08 MPa at a displacement rate of 1 mm s^{-1} and 6.06 MPa at 10 mm s^{-1}. While our values are slightly higher than those previously reported, this can be attributed to the fact that our analysis focuses solely on the DL behavior at higher displacement rates.

As shown in our results (Fig. 4), the DL exhibits greater stiffness at the upper and lower levels of the cervical spine at a displacement rate of 10 mm s^{-1}, while being stiffer at the C2-C5 levels at displacement rates of 0.1 and 1 mm s^{-1}. Variations in the tensile mechanical properties

across different cervical spinal levels have also been highlighted by Polak et al. (2014). These results can be interpreted in light of the varying amplitude of moment in the cervical segment, particularly in the caudal direction. Lower elastic modulus values indicate increased deformability and flexibility, which may help explain the observed trends.

The presented FE DL model is providing insights on the possibility to simulated the ligament in whole spine modelling. The von mises stresses distributions as well as strain-stress curves depict the differences between the three materials while failing to explain the trilinear behavior highlighted in the experimental results. It shows the necessity to model DL when simulated spinal cord quasi-static motions of the spine with spinal pia and dura maters. Improvement of such model could include simulation of continuous collagen fiber as well as better consideration of the pia and dura maters materials.

The trilinear behavior identified in our study raises important questions. If this behavior were observed only at higher displacement rates, one might assume that during dynamic traction, the DL would lack sufficient time to densify, resulting in decreased flexibility and requiring more force for greater displacement. This phenomenon could impair the dissipation or absorption of energy during traumatic events, leading to increased damage. However, our study demonstrates through ROC analysis that displacement rate should not be considered the sole factor that triggered trilinear behavior, as indicated by the high sensitivity and low specificity observed. These findings should be incorporated into finite element modeling of the DL. The specific behavior of the DL, depending of the application, and the influence of these changes warrant further numerical investigation.

The observed trilinearity of the stress-strain curve may be attributed to the differences in displacement rates applied during preconditioning and testing phases. The preconditioning phase was relatively slow, set at 0.125 Hz with an elongation of 1 mm, while the testing displacement rates ranged from 0.1 mm s^{-1} to 10 mm s^{-1} for samples with a total length of around 15 mm (including the pia mater, DL, and dura mater). This difference in strain rates (up to 10^2 times higher) alongside the limited elongation may account for variations in response. This phenomenon could be related to the fiber organization within the tissue, potentially reflecting fiber alignment during early loading followed by subsequent fiber straightening. It is possible that the material did not have adequate time or sufficient space to properly align its fibers, resulting in the limitations observed in the initial segment of the curve. The native crimped pattern of collagen fibers, as described in the microstructural analysis of denticulate ligaments by Ceylan et al. (2012), has also been reported to disappear under uniaxial load in other collagenous soft tissues, such as the dura mater and fascia lata (Szotek et al., 2021). The authors noted that this crimped pattern serves as a buffer against fiber damage and reemerges once the load or stretch ceases. But further microstructural investigation is required to confirm these findings. Additionally, the trilinear response could be influenced by the contributions of the dura mater and the pia mater. However, to the best of our knowledge, no trilinear stress-strain behavior has been reported in the testing of meningeal tissues.

Given these observations, the role of the DL in supporting the spinal cord as an attachment between the pia mater and the dura/arachnoid membranes within the vertebral foramen - under both physiological and traumatic conditions - should be reconsidered from a biomechanical perspective. Numerical models often overlook DL structures due to a lack of experimental data. Furthermore, realistic experimental testing of the SC is complicated by challenges in preserving cerebrospinal fluid during the testing process. Our study, which investigates three displacement rates across a spectrum of potential loading conditions, represents a preliminary step towards establishing material properties for use in numerical simulations. Future numerical studies should further explore the effects of the denticulate ligaments on the biomechanics of the cervical spine, taking into account their specific material properties and the variations observed across cervical levels.

4.1. Limitations

This study has several limitations. The in vitro nature of the research may influence the results as the DL were not tested at body temperature or in their natural environment.

Additionally, since the tests were conducted at constant displacement rates rather than constant strain rates, the approach to identifying a pivoting strain rate is both novel and limited. Indeed, a broader range of strain rates could have provided a more detailed analysis.

Although the stress-strain curves did not exhibit any inflection points or noticeable changes in slope, even at high strain rates, and that no plastic deformation were visually observed on sample following tensile testing, the possibility of minor plastic deformation cannot be entirely excluded. This potential effect on subsequent test results cannot be entirely ruled out and should be considered when interpreting the mechanical response of the samples.The exact strain rates applied to the pia mater and dura mater were not quantified using digital image correlation. Such analysis could have improved the accuracy of the DL strain calculation. Literature indicates that the boundaries between the DL and the pia mater, as well as between the DL and the dura mater, are not clearly defined. As a result, accurately determining the starting and ending points of the DL is difficult, given that fibers have been reported to insert into both the pia mater and the dura mater (Ceylan et al., 2012). Consequently, testing the DL as an independent component presents significant challenges.

5. Conclusion

In summary, our results indicate no significant differences in the material properties of the denticulate ligaments in the cervical region based on the applied displacement rate. The observed change in response - bilinear and trilinear – were only partially explain by displacement rate, with a strain rate threshold identified between the two response types. The data obtained are valuable for modeling the mechanical behavior of the SC along with the meninges and DL during traumatic events and quasi-static movements of the cervical spine. Future studies investigating the role of the pia mater and dura mater in the tensile testing of the DL would provide insight into their contributions to the elastic modulus and overall behavior of this complex. Additionally, further research could incorporate stress relaxation and dynamic mechanical analysis to more deeply characterize the viscoelastic behavior of denticulate ligaments.

CRediT authorship contribution statement

Audrey Berriot: Writing – original draft, Visualization, Validation, Methodology, Investigation, Formal analysis, Data curation, Conceptualization. **Morgane Evin:** Writing – review & editing, Writing – original draft, Resources, Project administration, Methodology, Investigation, Conceptualization. **Karim Kerkouche:** Visualization, Validation, Methodology, Formal analysis. **Elisabeth Laroche:** Methodology, Formal analysis, Data curation. **Eva Gerard:** Visualization, Software. **Eric Wagnac:** Writing – review & editing, Validation, Supervision, Project administration, Methodology, Investigation, Funding acquisition, Formal analysis, Data curation, Conceptualization.

Declaration of competing interest

The authors declare that they have no known competing financial interests or personal relationships that could have appeared to influence the work reported in this paper.

Appendix A. Supplementary data

Supplementary data to this article can be found online at https://doi.org/10.1016/j.jmbbm.2024.106824.

Data availability

Data will be made available on request.

References

Avril, S., Evans, S., Miller, K., 2013. Inverse problems and material identification in tissue biomechanics. J. Mech. Behav. Biomed. Mater. 27, 129–131. https://doi.org/10.1016/j.jmbbm.2013.07.001.

Beauséjour, M.-H., Wagnac, E., Arnoux, P.-J., Thiong, J.-M.M., Petit, Y., 2022. Numerical investigation of spinal cord injury after flexion-distraction injuries at the cervical spine. J. Biomech. Eng. 144, 011011. https://doi.org/10.1115/1.4052003.

Berriot, A., Wagnac, E., Laroche, E., Wei, W., Evin, M., 2023. Mechanical differences of anterior and posterior spinal nerve roots revealed by tensile testing. J. Biomech. 161, 111850. https://doi.org/10.1016/j.jbiomech.2023.111850.

Bilston, L.E., Thibault, L.E., 1995. The mechanical properties of the human cervical spinal cordIn Vitro. Ann. Biomed. Eng. 24, 67–74. https://doi.org/10.1007/BF02770996.

Ceylan, D., Tatarlı, N., Abdullaev, T., Şeker, A., Yıldız, S.D., Keleş, E., Konya, D., Bayri, Y., Kılıç, T., Çavdar, S., 2012. The denticulate ligament: anatomical properties, functional and clinical significance. Acta Neurochir. 154, 1229–1234. https://doi.org/10.1007/s00701-012-1361-x.

Czyz, M., Tykocki, T., Miękisiak, G., Ścigała, K., Będziński, R., Jarmundowicz, W., 2016. Critical values of mechanical stress and strain during traumatic cervical spinal cord injury: Clinical study with the use of Finite Element Modelling. J. Biomed. Graph. Comput. 6, 22. https://doi.org/10.5430/jbgc.v6n2p22.

Doehring, T.C., Carew, E.O., Vesely, I., 2004. The effect of strain rate on the viscoelastic response of aortic valve tissue: a direct-fit approach. Ann. Biomed. Eng. 32, 223–232. https://doi.org/10.1023/B:ABME.0000012742.01261.b0.

Erbulut, D.U., Zafarparandeh, I., Lazoglu, I., Ozer, A.F., 2014. Application of an asymmetric finite element model of the C2-T1 cervical spine for evaluating the role of soft tissues in stability. Med. Eng. Phys. 36, 915–921. https://doi.org/10.1016/j.medengphy.2014.02.020.

Evin, M., Sudres, P., Weber, P., Godio-Raboutet, Y., Arnoux, P.-J., Wagnac, E., Petit, Y., Tillier, Y., 2022. Experimental Bi-axial tensile tests of spinal meningeal tissues and constitutive models comparison. Acta Biomater. 140, 446–456. https://doi.org/10.1016/j.actbio.2021.11.028.

Fung, Y.C., 1984. Structure and stress-strain relationship of soft tissues. Am. Zool. 24, 13–22.

Greaves, C.Y., Gadala, M.S., Oxland, T.R., 2008. A three-dimensional finite element model of the cervical spine with spinal cord: an investigation of three injury mechanisms. Ann. Biomed. Eng. 36, 396–405. https://doi.org/10.1007/s10439-008-9440-0.

Jackson, A.B., Dijkers, M., DeVivo, M.J., Poczatek, R.B., 2004. A demographic profile of new traumatic spinal cord injuries: change and stability over 30 years. Arch. Phys. Med. Rehabil. 85, 1740–1748. https://doi.org/10.1016/j.apmr.2004.04.035.

Kang, W., Zhang, Y., Bu, W., Zhao, Y., Wang, L., Liu, S., 2023. Statistical analysis of mechanical properties of biological soft tissue under quasi-static mechanical loading. Medicine in Novel Technology and Devices 17, 100202. https://doi.org/10.1016/j.medntd.2022.100202.

Kumar, R., Lim, J., Mekary, R.A., Rattani, A., Dewan, M.C., Sharif, S.Y., Osorio-Fonseca, E., Park, K.B., 2018. Traumatic spinal injury: global epidemiology and worldwide volume. World Neurosurgery 113, e345–e363. https://doi.org/10.1016/j.wneu.2018.02.033.

Marino, M., 2018. Constitutive modeling of soft tissues. https://doi.org/10.1016/B978-0-12-801238-3.99926-4.

Parkinson, D., 1991. Human spinal arachnoid septa, trabeculae, and ?rogue strands? Am. J. Anat. 192, 498–509. https://doi.org/10.1002/aja.1001920414.

Polak, K., Czyż, M., Ścigała, K., Jarmundowicz, W., Będziński, R., 2014. Biomechanical characteristics of the porcine denticulate ligament in different vertebral levels of the cervical spine—preliminary results of an experimental study. J. Mech. Behav. Biomed. Mater. 34, 165–170. https://doi.org/10.1016/j.jmbbm.2014.02.010.

Polak-Kraśna, K., Robak-Nawrocka, S., Szotek, S., Czyż, M., Gheek, D., Pezowicz, C., 2019. The denticulate ligament – tensile characterisation and finite element micro-scale model of the structure stabilising spinal cord. J. Mech. Behav. Biomed. Mater. 91, 10–17. https://doi.org/10.1016/j.jmbbm.2018.11.017.

R Core Team, 2020. R: A Language and Environment for Statistical Computing. R Foundation for Statistical Computing, Vienna, Austria.

Rycman, A., McLachlin, S.D., Cronin, D.S., 2022. Spinal cord boundary conditions affect brain tissue strains in impact simulations. Ann. Biomed. Eng. https://doi.org/10.1007/s10439-022-03089-7.

Singhal, I., Harinathan, B., Warraich, A., Purushothaman, Y., Budde, M.D., Yoganandan, N., Vedantam, A., 2023. Finite element modeling of the human cervical spinal cord and its applications: a systematic review. N Am Spine Soc J 15, 100246. https://doi.org/10.1016/j.xnsj.2023.100246.

Stoner, K.E., Abode-Iyamah, K.O., Magnotta, V.A., Howard, M.A., Grosland, N.M., 2019. Measurement of in vivo spinal cord displacement and strain fields of healthy and myelopathic cervical spinal cord. J. Neurosurg. Spine 31, 53–59. https://doi.org/10.3171/2018.12.SPINE18989.

Sudres, P., Evin, M., Wagnac, E., Bailly, N., Diotalevi, L., Melot, A., Arnoux, P.-J., Petit, Y., 2021. Tensile mechanical properties of the cervical, thoracic and lumbar porcine spinal meninges. J. Mech. Behav. Biomed. Mater. 115, 104280. https://doi.org/10.1016/j.jmbbm.2020.104280.

Szotek, S., Dawidowicz, J., Geniusz, M., Kozak, M., Łukomski, R., Czogalla, A., 2021. The biomechanical characteristics of spinal dura mater in the context of its basic morphology. Acta Bioeng. Biomech. 23, 149–159.

Tran, D.T., Tsai, L., 2023. Effect of strain rates on the mechanical response of whole muscle bundle. J. Biol. Phys. 49, 257–267. https://doi.org/10.1007/s10867-023-09630-6.

Tubbs, R.S., Salter, G., Grabb, P.A., Oakes, W.J., 2001. The denticulate ligament: anatomy and functional significance. J. Neurosurg. Spine 94, 271–275. https://doi.org/10.3171/spi.2001.94.2.0271.